

Applying Activated Carbon Derived from Coconut Shell Loaded by Silver Nanoparticles to Remove Methylene Blue in Aqueous Solution

Huu Tap Van · Thi Minh Phuong Nguyen ·
Vu Thi Thao · Xuan Hoa Vu · Tien Vinh Nguyen ·
Lan Huong Nguyen

Received: 10 September 2018 / Accepted: 15 November 2018 / Published online: 26 November 2018
© Springer Nature Switzerland AG 2018

Abstract This study developed a new adsorbent, specifically activated carbon-loaded silver nanoparticles (AgNPs-AC) by coating the silver nanoparticles (AgNPs) onto activated carbon (AC). The obtained AgNPs-AC were characterized by scanning electron microscopy (SEM), energy-dispersive spectrometry (EDS), Fourier transform infrared spectroscopy (FTIR), and Brunauer-Emmett-Teller (BET). The ability of

AgNPs-AC to remove methylene blue (MB) was evaluated using different experimental factors, these being pH solution, contact time, adsorbent dose, and initial MB concentration. Results indicated that the highest adsorption capacity of MB onto AgNPs-AC was obtained when the AC was loaded onto AgNPs at the impregnation ratio of 0.5% w/w for AC and AgNPs. The best conditions in which AgNPs-AC could remove MB were as follows: pH 10, contact time lasting 120 min, and adsorbent dose being 250 mg/25 mL solution. In this scenario, the maximum adsorption capacity of MB onto AgNPs-AC was 172.22 mg/g. The adsorption isothermal equilibrium was well described by the Langmuir, Freundlich and Sips models. The Sips equations had the highest correlation coefficient value ($R^2 = 0.935$). The pseudo-first-order and pseudo-second-order kinetic models agree well with the dynamic behavior of the adsorption of dye MB on AgNPs-AC.

H. T. Van
Faculty of Resources and Environment, Thai Nguyen University of Sciences (TNUS), Tan Thinh Ward, Thai Nguyen, Vietnam

T. M. P. Nguyen
Faculty of Environment and Chemical Engineering, Duy Tan University (DTU), 254 Nguyen Van Linh Road, Da Nang, Vietnam

V. T. Thao
Advanced Education Program Office, Thai Nguyen University of Agriculture and Forestry (TUA), Quyet Thang Ward, Thai Nguyen City, Vietnam

X. H. Vu
Faculty of Physics and Technology, Thai Nguyen University of Sciences (TNUS), Tan Thinh Ward, Thai Nguyen City, Vietnam

T. V. Nguyen
Faculty of Engineering and IT, University of Technology Sydney (UTS), Box 123, Broadway, Sydney, PO, Australia

L. H. Nguyen (✉)
Faculty of Environment – Natural Resources and Climate Change, Ho Chi Minh City University of Food Industry (HUFI), 140 Le Trong Tan Street, Tay Thanh Ward, Tan Phu District, Ho Chi Minh City, Vietnam
e-mail: lanhuongba@gmail.com

Keywords Silver nanoparticle · Activated carbon · AgNPs-AC · Methylene blue · Adsorption

1 Introduction

Discharging levels of organic compounds originating from human activities into water bodies generally does great harm to living organisms. Dyes exist in these organic compounds and they constitute one of the most serious environmental problems due to their high toxicity and color. The dyes are used widely in various industries such as textiles, rubber, carpets, paper,

printing, and plastics (Sara and Tushar 2014; Shu et al. 2015). The discharge of dyes into water sources leads to many serious environmental and health problems (Hamadi et al. 2017). Most of the dye causes water colorization at very low concentrations which consequently result in serious ecological problems, destroy aquatic organisms, and harm human health (Chen et al. 2018; Stoyanova and Christoskova 2011). The most widely used dye is methylene blue (MB) which serves as a chemical agent for dyeing cotton, wood, and silk (Rafatullah et al. 2010). It can stimulate and permanently injure the eyes of human and animals (Rafatullah et al. 2010). Also, eating foods contaminated with MB leads to nausea, vomiting, profuse sweating, mental confusion, and methemoglobinemia (Ghosh and Bhattacharyya 2002; Tan et al. 2008a, b). For these reasons, it is vital to remove MB from wastewater effluents before discharging them into water bodies so that its harmful impacts on receiving waters can be minimized as much as possible.

In the past decades, to treat wastewater contaminated by MB, numerous conventional treatment techniques including oxidation, electrochemical oxidation, biological treatment, coagulation, and adsorption have been applied (De Castro et al. 2018). Of the existing techniques, adsorption has been acknowledged as the most economical, with its simple operation and high efficient method in removing organic compounds from wastewater. Commercial high-quality activated carbon (AC) can be used to remove MB from wastewater effluents due to its high-adsorption capacity. However, it has not been used widespread due to its relatively high cost. Thus, recent studies tend to advocate the development of low-cost adsorbents for MB removal. These include agricultural wastes, industrial solid wastes, biomass, clay minerals and zeolites, and their modified materials to improve adsorption capacity (Tran et al. 2015; Vu et al. 2017). Hence, cost-effective commercial activated carbon can also be produced from agricultural wastes such as coconut shells (Benaouda et al. 2008; El Qada et al. 2008; Raposo et al. 2009).

Recent advances in nanotechnology have not only created a breakthrough in electronics (Kritika et al. 2010), informatics, and biomedical technology (Ganau et al. 2018), but are now widely applied in other aspects of life. Nanomaterials have excellent motorized and physical properties due to their extremely fine grain size and high grain boundary volume fraction (Krishnananda et al. 2017). Among these nanomaterials, silver

nanoparticles (AgNPs) have been used extensively in therapeutic applications as catheters, surgical devices and wound dressings (Tang et al. 2017), and environmental applications, for example, antibacterial character by interacting with cell membranes of pathogens in water (Sharma and Sharma 2010). Nonetheless, the production of AgNPs is an expensive exercise and has discouraged its application in wastewater treatment.

To improve the adsorption capacity of commercial activated carbon, many studies concentrated on modifying cost-effective AC with various chemicals, such as H_3PO_4 (Fierro et al. 2006), H_2SO_4 (Singh et al. 2008), $ZnCl_2$ (Yorgun et al. 2009), HNO_3 (Lopes et al. 2015), and $NaOH$ (Vu et al. 2017). However, to the best of our knowledge, no study has yet been done on combining activated carbon and silver nanoparticles to produce a new modified material for removing dyes from aqueous solution. With a huge surface area and proper microspore, activated carbon is an ideal supporting material for loading AgNPs (Abe et al. 2000; Chingombe et al. 2006; Tang et al. 2017). This study, therefore, investigated the coating of AgNPs on the AC and evaluated the new adsorbent's capacity to remove MB from aqueous solution. To attain this objective, the silver nanoparticles were directly loaded onto the activated carbon derived from coconut shell to produce AgNPs-AC. The physicochemical properties and adsorption mechanisms of MB on AgNPs-AC were studied through analyses comprising scanning electron microscopy (SEM), energy-dispersive spectrometry (EDS), Fourier transform infrared spectroscopy (FTIR), Brunauer-Emmett-Teller (BET), and batch experiments.

2 Materials and Methods

2.1 Materials

MB with the chemical formula of $C_{16}H_{18}C_1N_3S \cdot 3H_2O$ was purchased from Merck. The stock MB solution (1000 mg/L) was prepared by dissolving 1.0 g MB in 1000 mL of distilled water. All working solutions were obtained by diluting the stock solution with distilled water to the desired concentrations.

2.2 Synthesis of Silver Nanoparticles

Silver nitrate ($AgNO_3$) was used as the precursor to create silver nanoparticles. Silver nanoparticles

(AgNPs) were prepared by the hydrothermal method (Tang et al. 2017). Firstly, 100 mL of AgNO_3 solution (0.001 M) was mixed with 0.2 g of starch to generate starch solutions containing Ag^+ ions. Then, the solution was stirred vigorously on a magnetic stirrer at 70 °C to ensure the homogeneous nature of the mixture. The temperature of the solution was continuously maintained at 70 °C and 25 ml of sodium borohydrides (0.001 M) was gradually added (drop by drop) into the mixture. Finally, the resultant solution was cooled to room temperature for further usage (Mulfinger et al. 2007).

2.3 Preparation of the AgNPs-Loaded Activated Carbon

Commercial granular activated carbon (AC) with particle size from 1 to 2 cm was purchased from Tra Bac Company, Vietnam. The AC was ground and sieved to obtain particle size less than 0.5 mm. The AC was then washed and dried at 105 °C for 2 h in an oven.

The impregnation method was used to load AgNPs on AC. The mixture of AC with AgNPs was carried out at various mass ratio (0.5–1.5% w/w of AC and AgNPs) by using the incipient wet-impregnation technique in flasks. The flasks were then shaken at 120 rpm orbital for 24 h in the dark (AbdEl-Salam et al. 2017). After impregnation, the wet samples were filtered and dried for 2 h at 105 °C to obtain modified AC (AgNPs-AC). The AgNPs-AC with average particle size less than 0.5 mm was used in the batch-mode adsorption experiments to remove MB from aqueous solution.

2.4 Characterization of AgNPs-AC

The morphologies of AC and AgNPs-AC were determined by energy dispersive X-ray spectroscopy (Hitachi S-4800) with EDS and SEM systems. The crystalline structures of AgNPs-AC were examined by X-ray diffraction pattern using XRD-D8 ADVANCE, with the Cu K α radiation ($\lambda = 1.5417 \text{ \AA}$). The scan angle covered $15^\circ < 2\theta < 70^\circ$ at a scan speed of $3^\circ/\text{min}$. The presence of surface functional groups of AgNPs-AC was detected using Fourier transform infrared spectroscopy (FT/IR-6300) in the $4000\text{--}500 \text{ cm}^{-1}$ range. The pH at the point of zero charge (pH_{PZC}) was determined by the drift method (Tran et al. 2015). BET surface area of AC before and after AgNPs loading was measured by a pore size and specific surface area analyzer (BET, Builder, SSA-4300).

2.5 Batch Adsorption Experiments

Adsorption experiments of MB onto AgNPs-AC were conducted utilizing the batch mode. The experiments were conducted in batch flasks containing desired weights of adsorbent (AgNPs-AC) and 25 mL of MB solution. The mixture was gently stirred at a speed of 120 rpm in 100-mL conical flasks. The experimental conditions for investigating the effects of impregnation ratio, pH medium, adsorbent dosage, contact time, and initial concentrations of MB on adsorption capacity of AgNPs-AC are presented in Table 1. Here, the pH of solution was adjusted employing 0.1 M NaOH and 0.1 M HCl solutions.

2.6 Measurements

The suspensions from batch experiments were filtered (through Whatman No. 1 filter paper, pore size $0.22 \mu\text{m}$). The concentration of MB in the filtrates was measured through COD value via the bicromate standard methods (Rice et al. 2012). pH of solution was measured by Hanna HI 9025 pH meter.

The MB removal efficiency (%) was calculated using the following equation:

$$\% \text{removal} = \frac{(C_i - C_t)^*}{C_i} 100 \quad (1)$$

where C_i is the initial concentration (mg/L) and C_t is the concentration (mg/L) at any time t .

Adsorption capacity at time t , q_t (mg/g) was obtained as follows:

$$q_t = \frac{C_i - C_t^*}{m} V \quad (2)$$

where V (L) is the volume of the solution and m (g) is the mass of AgNPs-AC.

Adsorption capacity at equilibrium, q_e (mg/g) was calculated using

$$q_e = \frac{C_i - C_e^*}{m} V \quad (3)$$

where C_e (mg/L) is the equilibrium concentration.

2.7 Data Analysis

All experiments were done in triplicate. All data statistics, comprising means, standard deviations, relative

Table 1 Summary of experimental conditions of adsorption of MB onto AgNPs-AC

Investigated parameter	Temperature (°C)	pH	AgNPs-AC dosage (mg)	Contact time (min)	Initial conc. of MB (mg/L)	Impregnation ratio (%)
Impregnation ratio (%)	25	5	50	60	500	0–1.5
pH	25	2–12	50	60	500	0.5
Contact time (min)	25	10	50	0–180	500	0.5
AgNPs-AC dose (mg)	25	10	50–500	120	500	0.5
Initial conc. of MB (mg/L)	25	10	250	120	100–1000	0.5

standard deviations, and regressions (linear) were computed on SPSS software version 19.0. Wherever possible, the error bars indicating the standard deviation are illustrated in all figures.

2.8 Adsorption Isotherm Models

The equilibrium adsorption isotherms need to be built to describe the relationship between adsorbate and adsorbent so that the adsorption mechanism can be identified. In this study, adsorption isothermal equilibrium of methylene blue on AgNPs-AC was described by the Langmuir, Freundlich, and Sips models. The Langmuir sorption isotherm is applied to equilibrium sorption assuming monolayer sorption onto a surface with a finite number of identical sites (Pathania et al. 2017). The Langmuir model can be expressed as the following equation:

$$q_e = \frac{q_m b C_e}{1 + b C_e} \quad (4)$$

where C_e is the equilibrium concentration in liquid phase (mg/L), q_m is the monolayer adsorption capacity (mg/g), and b is the Langmuir constant related to the free adsorption energy (L/mg).

Heterogeneous surface energy systems can be described by the Freundlich model (Dada et al. 2012). The following equation represented the Freundlich method:

$$q_e = K_F C_e^{1/n} \quad (5)$$

where K_F is a constant, indicating the adsorption capacity of the adsorbent (mg/g) while constant $1/n$ is the intensity of the adsorption.

The Sips model is a combination of the Langmuir and Freundlich isotherm models. The equation describes Sips isotherm model as follows:

$$q_e = \frac{q_m (b C_e)^{1/n}}{1 + (b C_e)^{1/n}} \quad (6)$$

2.9 Adsorption Kinetics

Pseudo-first-order, pseudo-second-order, and Elovich models were used to investigate the MB adsorption kinetics on AgNPs-AC. The linear forms of pseudo-first-order, pseudo-second-order, and Elovich equations are presented as follows, respectively:

$$\ln(q_e - q_t) = \ln q_e - k_1 t \quad (7)$$

$$\frac{t}{q_t} = \frac{1}{k_2 q_e^2} + \frac{1}{q_e} t \quad (8)$$

$$q_t = \beta \ln(\alpha \beta t) \quad (9)$$

where the adsorption rate (k_1) is calculated by linear regression analysis of the pseudo-first-order model from the slope of linear plot of experimental data; k_2 is the constant of pseudo-second-order rate; q_e is the sorption capacity at equilibrium; q_t is the adsorption capacity at time t ; α is the initial adsorption rate (mg/g min); and β is the adsorption constant (g/mg).

3 Results and Discussion

3.1 Characterization of Activated Carbon-Loaded Silver Nanoparticles

The porous surface structure is one of the features affecting the adsorption capacity of AC. Analysis results

of nitrogen adsorption/desorption isotherm (data not showed) showed that AC has a porous surface structure (Fig. 1a) with high Brunauer–Emmett–Teller (BET) specific surface area of 691.64 m²/g and total pore volume of 0.062 cm³/g. After the AC was impregnated with silver nanoparticles (AgNPs-AC) at the ratio of 0.5% w/w of AC and AgNPs, the surface morphology of AgNPs-AC was observed to clearly change in terms of SEM (Fig. 1b). More specifically, it contained a porous structure with a small difference in surface area (S_{BET} of 705.32 m²/g) and total pore volume (0.065 cm³/g). Figure 1b indicates that silver nanoparticles were successfully loaded onto activated carbon.

The EDS analysis (Fig. 1c) revealed that AC is mainly composed of C (91.87%) and O (8.13%) elements. However, a AgNP was recognized in the EDS analysis of AgNPs-AC (Fig. 1d) where the proportions of elements for C, O, and Ag were 80.51%, 19.42%, and 0.07%, respectively. In this case, the silver nanoparticles were successfully attached to the AC surface leading to improved methylene blue adsorption capacity of AC.

Additionally, the XRD spectra of AC (Fig. 2a) and AgNPs-AC (Fig. 2b) indicated that almost all characteristic peaks were well indexed to amorphous with a highly graphite crystal structure. The graph showed that the broad peak occurred at 30.09° and 61.93° with the AC (Fig. 2a) and at 22.63° with AgNPs-AC (Fig. 2b). The results revealed that the activated carbon is carbon graphite. The presence of Ag on the AC's surface at the peak of 43.86° in the case AgNPs-AC (Fig. 2b) confirmed that AgNPs were loaded onto the AC. Similar results were obtained recently by Altintig et al. (2016) when notable peaks in mixtures of activated carbon and silver nanoparticles were evident at the peak of 44° in XRD spectra. Similarly, Abdel-Salam et al. (2017) discovered that in their work on the adsorption of crystal violet, AgNPs appeared at the peak of 37.9° when loading AgNPs onto AC.

Quantitative information regarding the dominant functional groups on the AC, AgNPs-AC surface were provided by FTIR spectra and presented in Fig. 3. The broad peaks at 3822, 3720, and

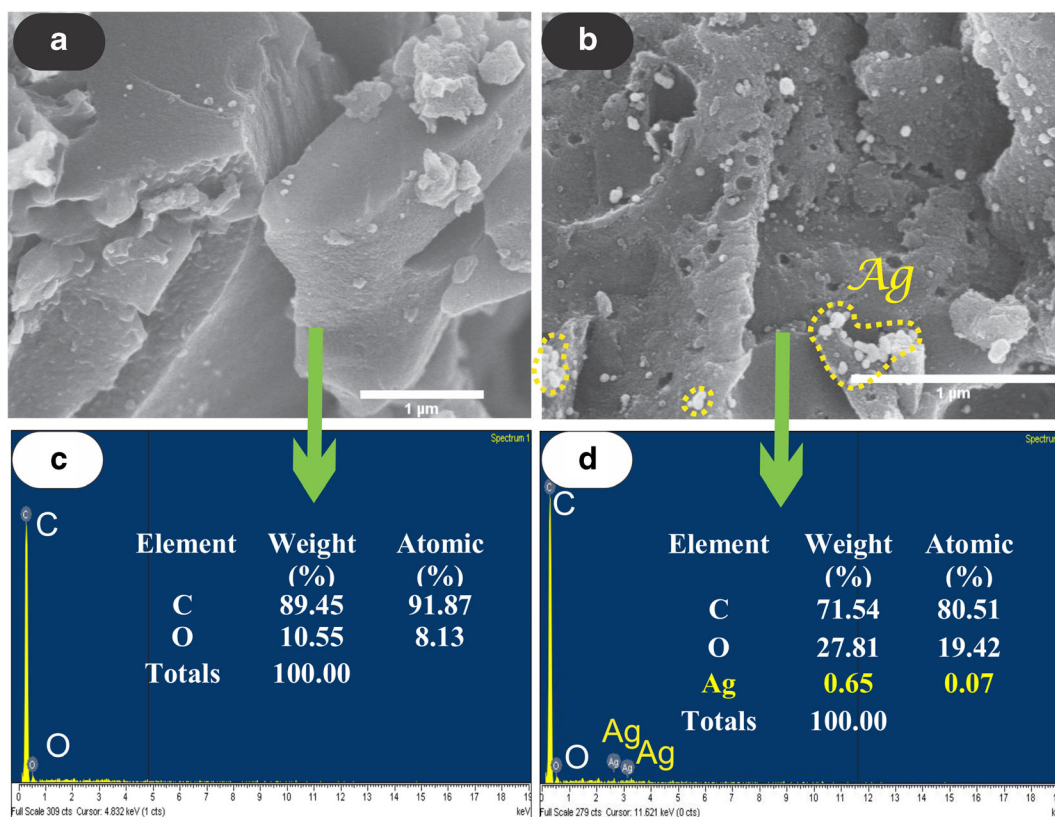
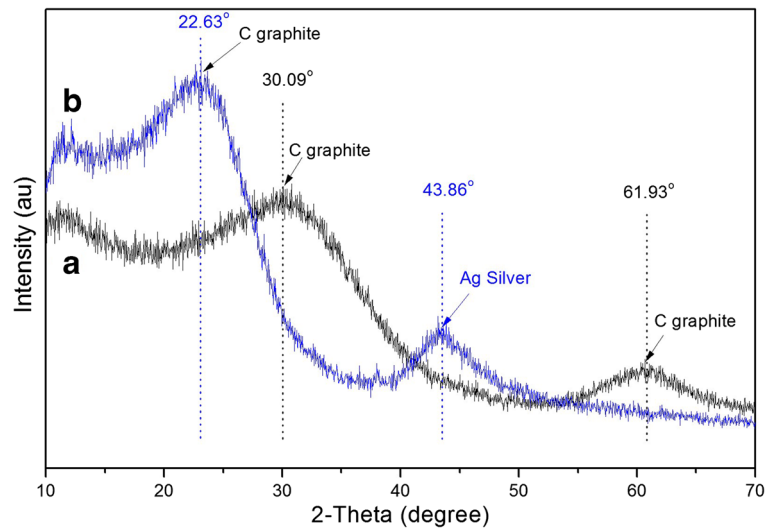


Fig. 1 SEM image of **a** AC and **b** activated carbon-loaded AgNPs (AgNPs-AC), EDS spectra of **c** AC and **d** activated carbon-loaded AgNPs (AgNPs-AC)

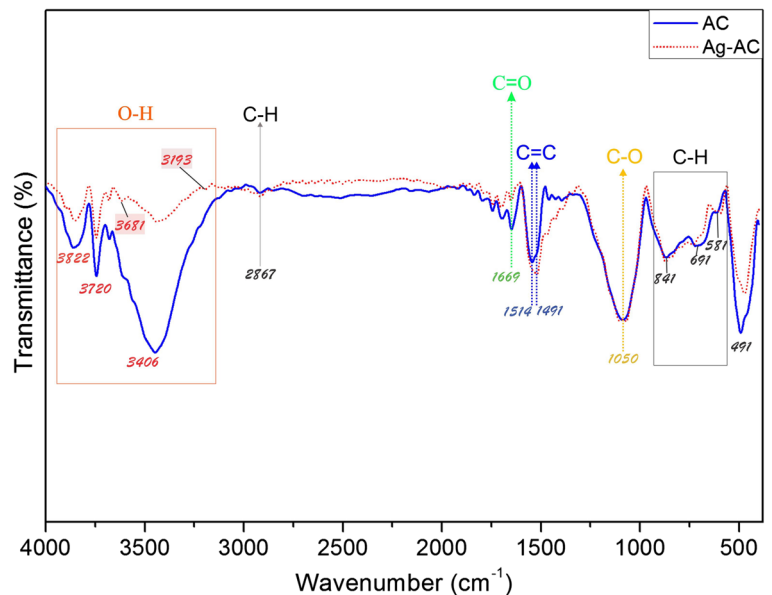
Fig. 2 XRD graph of **a** activated carbon from coconut shells (AC) and **b** activated carbon-loaded AgNPs (AgNPs-AC)



3406 cm^{-1} and two peak appeared at 3681 and 3193 cm^{-1} on AgNPs-AC, confirming the presence of O–H stretch bonded group. A peak at around 3200–3800 cm^{-1} suggested the existence of O–H group (Anisuzzaman et al. 2015; De Castro et al. 2018). For AC-loaded AgNPs (AgNPs-AC), the peak became narrower at 3406 cm^{-1} and had a new peak in comparison to AC. This shows that Ag^+ ions joined the activated carbon surfaces (Altintig et al. 2016). A small peak at around 1669 cm^{-1} highlighted the existence of C=O stretching vibration in carbonyls,

these being ketones, aldehydes, lactones, and carboxylic groups (Altintig et al. 2016; Anisuzzaman et al. 2015). The peak of 1514 cm^{-1} (for AC) and its shift to 1491 cm^{-1} (for AgNPs-AC) demonstrated the C=C stretching vibration in aromatic rings (Foo and Hameed 2009) with a broader band due to the presence of AgNPs. A strong peak of 1050 cm^{-1} frequency indicated C–O stretching of carboxylic acids or lactone groups. Similar results have been documented elsewhere (Altintig et al. 2016; Lazim et al. 2015). The presence of aromatic –C–H out-of-plane bending

Fig. 3 FTIR graph of AC and AgNPs-AC



in benzene derivatives was evident at 581–841 cm^{-1} (Anisuzzaman et al. 2015).

3.2 Effect of Impregnation Ratio of AgNPs and AC (AgNPs/AC) on Methylene Blue Adsorption

Initial experiments were carried out to compare adsorption capacity of AC with AgNPs-AC. AgNPs-AC was prepared by soaking AC in the above silver nanoparticles with different impregnation ratios, from 0 to 1.5% w/w of AgNPs and AC.

From Fig. 4, it is clear that the adsorption capacity (q) of AgNPs-AC for MB was much higher than that of AC. The adsorption capacity was 38.89 mg/g for AC while it was 61.11–84.81 mg/g for AgNPs-AC with impregnation ratio of silver nanoparticles and activated carbon w/w decreasing from 1.5 to 0.5%. The highest capacity reached 84.81 mg/g (with MB removal percentage being 33.93%) at the impregnation ratio of 0.5%. This improvement can be explained by the silver nanoparticles loaded on AC increasing their active functional groups (peak of 3681 cm^{-1} and 3193 cm^{-1} in Fig. 3) compared to the original AC. However, the adsorption capacity declined remarkably when the impregnation ratio of AC in AgNPs rose from 1 to 1.5%. The explanation for this may be that the active sites on AgNP surfaces were saturated and there were not enough active sites for MB attachment onto AgNPs-AC (Nguyen et al. 2015). Based on the above results, the adsorption capacity of AgNPs-AC reached its maximum at the impregnation ratio between AC and AgNPs (w/w) of 0.5%. Consequently, the impregnation ratio of 0.5%

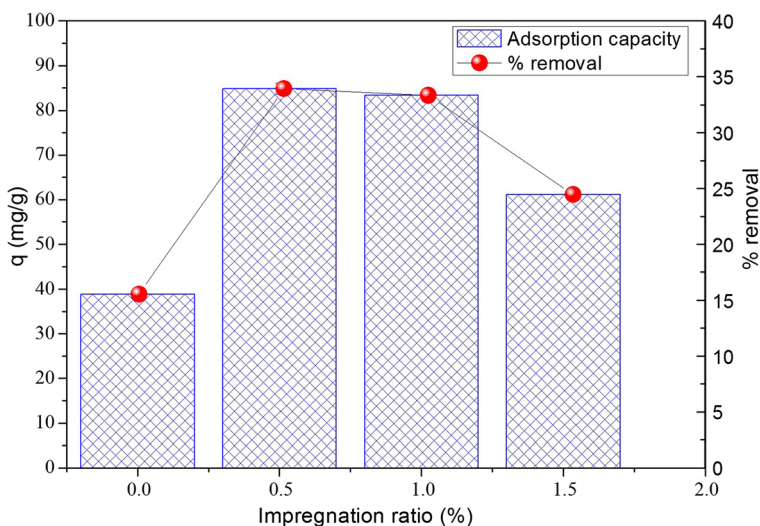
emerged as the most suitable for subsequent experiments.

3.3 Effect of pH

The pH of the dye solution plays an important role in adsorption capacity because it affects both the degree of ionization of the dye as well as the surface properties of the adsorbent (Özbay et al. 2013). To investigate the effects of pH solution on the sorption of MB, an experiment was conducted at various pH levels, ranging from 2.0 to 12.0. The initial MB concentration, contact time, and dose of AgNPs-AC were fixed at 500 mg/L, 60 min, and 50 mg/25 mL, respectively.

Figure 5 shows that the adsorption capacities of AgNPs-AC and efficiency in removing MB were pH-dependent. An increase in $\text{pH}_{\text{solution}}$ from 2 to 10 led to a significant increase in adsorbed amount of MB onto AgNPs-AC as well as removal efficiency of MB. The adsorption capacity and MB removal efficiency reached the maximum values of 149.64 mg/g and 60% at $\text{pH}_{\text{solution}}$ 10, respectively. When pH ranged between 11 and 12, adsorption capacity and removal efficiency of MB decreased slightly, reaching 120 mg/g and 56%, respectively. The pH_{pzc} of AC and AgNPs-AC before the adsorption process were found to be 4.13 and 5.03, respectively, and was 4.91 for AgNPs-AC following the adsorption process. These results indicated that pH_{pzc} of AgNPs-AC was similar. At $\text{pH}_{\text{solution}} < \text{pH}_{\text{pzc}}$, the surface of AgNPs-AC became positively charged. Competition between H^+ and positively charged MB cations for vacant adsorption sites triggered a reduction in MB

Fig. 4 Effect of impregnation ratio concerning AgNPs and AC on MB adsorption at initial concentration of MB, 500 mg/L; adsorbent dose, 50 mg AgNPs-AC/25 mL solution; and temperature, 25 °C



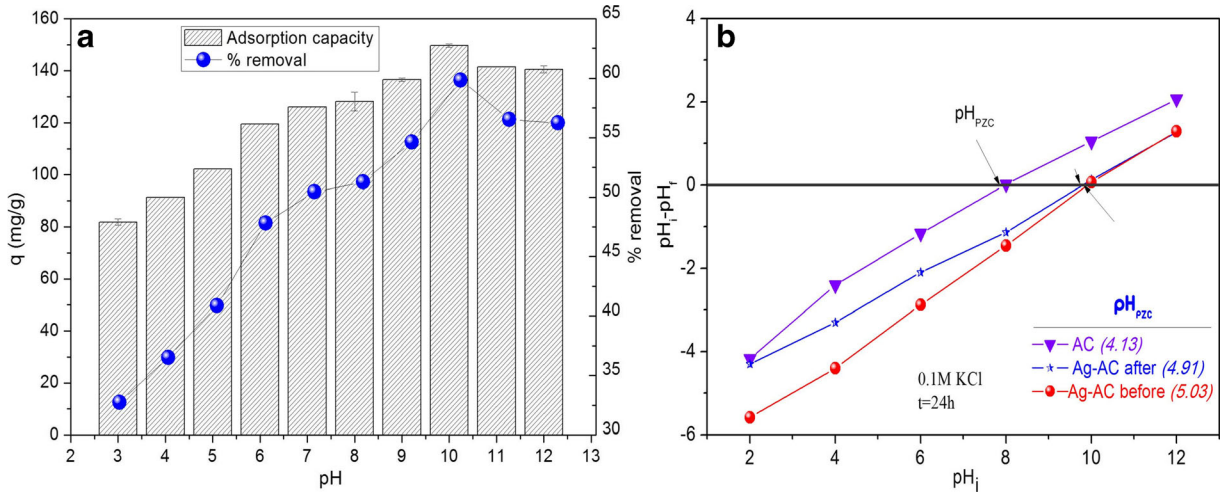


Fig. 5 a Effect of pH on MB adsorption at initial concentration of MB, 500 mg/L; adsorbent dose, 50 mg AgNPs-AC/25 mL solution; contact time, 60 min; temperature, 25 °C and b pH_{PZC} of AC, AgNPs-AC before and after adsorption of MB

uptake due to the large amount of H^+ ions (Kushwaha et al. 2014; Pathania et al. 2017). At the $pH_{solution} > pH_{PZC}$, the adsorbent surface was negatively charged by the OH^- ions. This resulted in an increase in the electrostatic interaction between the cationic MB and OH^- ions, which caused MB adsorption to increase. The results suggested that electrostatic attraction played a significant role in the adsorption mechanism of MB onto AgNPs-AC. The same results have been reported in other recent studies (Chen et al. 2018; Kushwaha et al. 2014; Pathania et al. 2017). They all reported that the adsorption mechanism of dye onto various activated

carbon-loaded nanoparticles was electrostatic attraction between adsorbent and adsorbate.

3.4 Effect of Contact Time

Determination of the equilibrium time plays an important role in designing wastewater treatment processes with adsorption (Vaipoulou and Gikas 2011). The effects of contact time on adsorption of MB onto AgNPs-AC were examined at various contact times (5–180 min) at $pH_{solution}$ of 10 to determine the equilibrium time.

Fig. 6 Effect of contact time on MB adsorption onto AgNPs-AC at pH 10, initial concentration of MB, 500 mg/L; adsorbent dose, 50 mg AgNPs-AC/25 mL solution; and temperature, 25 °C

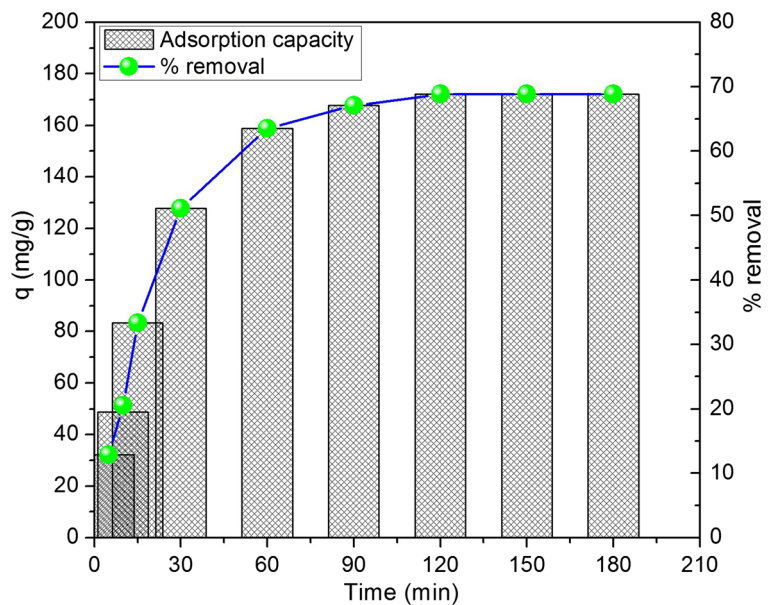


Fig. 7 Effect of AgNPs-AC dosage on MB adsorption at pH 10, contact time, 120 min; initial concentration of MB, 500 mg/L; temperature, 25 °C

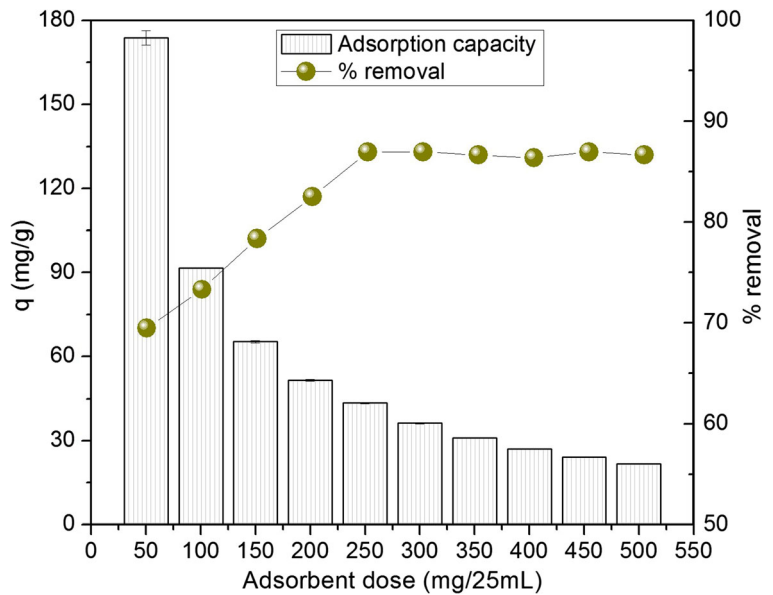


Figure 6 shows that a rapid adsorption can be seen at the initial stage of the contact periods (10–30 min). The adsorption capacity and removal efficiency of MB from 32.22 mg/g, and 12.89%, respectively, for the first 5 min increased quickly to 127.78 mg/g and 51%, respectively, for the next 30 min. This can be explained by the large number of available surface sites of the AgNPs-AC for adsorption of MB during the initial stage. However, the adsorption process continued slowly until it reached equilibrium at 120 min (adsorption capacity and removal efficiency of 172.22 mg/g and 69%, respectively). From

120 to 180 min, the adsorption process remained constant. It is clear that initially the capillary site of AgNPs-AC is large and the adsorption process began quickly. Over a period of time, the adsorption process reached saturation due to the lack of available active sites required for further uptake (Pathania et al. 2017) and unavailability or limited availability of active sites on the adsorbent (AbdEl-Salam et al. 2017). As a result, the adsorption efficiency became stable. This trend was similar to that reported by other researchers (El Alouani et al. 2018; Pathania et al. 2017; Salem et al. 2018).

Fig. 8 Effect of initial MB concentrations on the adsorption of MB by AgNPs-AC at pH 10, contact time, 60 min; adsorbent dose, 250 mg/25 mL; and temperature, 25 °C

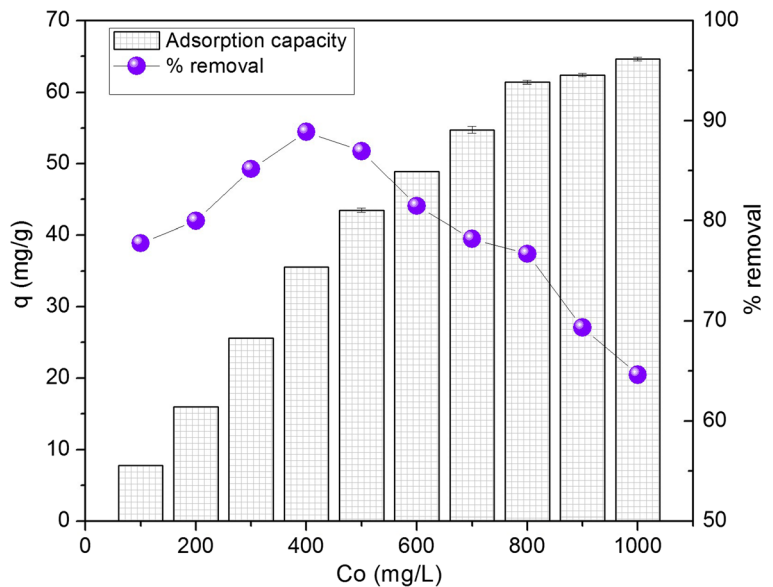
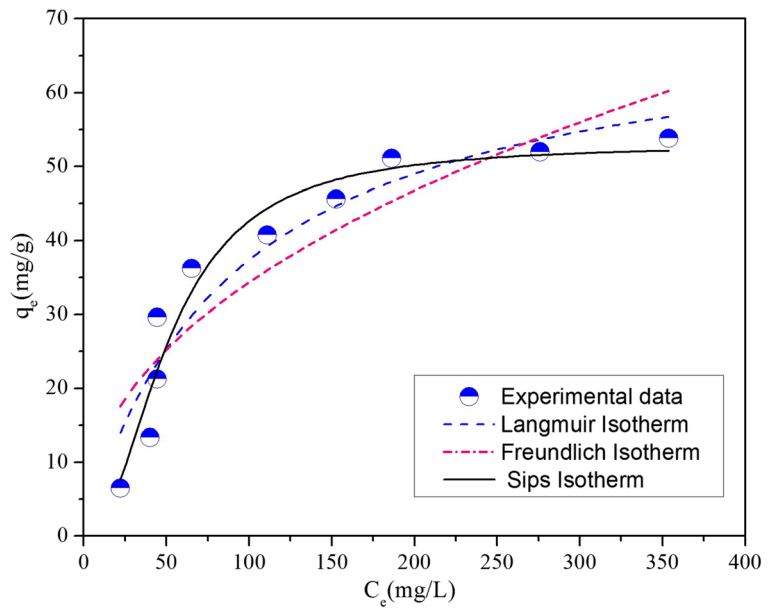


Fig. 9 Adsorption isothermal equilibrium prediction of MB onto AgNPs-AC at contact time of 120 min and AgNPs-AC dose of 250 mg/25 mL



3.5 Effect of Adsorbent Dose

Adsorbent dosage is an important parameter which affects adsorption capacity at a certain initial concentration of adsorbate (Tan et al. 2012). The effects of various AgNP-AC doses from 50 to 500 mg in 25 mL MB solution at optimum pH of 10 and the initial MB concentration of 500 mg/L on MB adsorption were investigated. The results are depicted in Fig. 7.

From Fig. 7, it can be seen that the adsorbent dosage can influence MB removal efficiency at a certain initial concentration of adsorbate. The results indicate that the removal efficiency of MB increased from 69.5 to 87.0% while adsorption capacity decreased, respectively, from 173.70 to 43.48 mg/g when increasing the dose of AgNPs-AC from 50 to 250 mg/25 mL solution. The maximum removal efficiency of MB was achieved at 87.0% at a dose of AgNPs-AC of 250 mg/25 mL solution. The adsorption efficiency of MB did not increase

and the adsorption capacity tended to decline slightly when the AgNPs-AC dose was more than 250 mg/25 mL solution. Based on this, it can be seen the adsorbent amount plays a significant role in the adsorption process of MB by AgNPs-AC. The removal percentage of MB increased when elevating the quantity of AgNPs-AC, which can be explained by the existence of a greater number of available active sites on the AgNP-AC surface. This eventuated in an increase in the active linkage sites participating in the adsorption (Salem et al. 2018). Our findings in this study indicated that AgNPs enhanced MB uptake onto AC and resulted in more efficient MB removal from aqueous solution. This was because AgNPs have a high surface area and unique structure characteristics; thus, the activated carbon-loaded AgNP active sites increased in number on the AC surface (Syu et al. 2014). This same trend has been documented in other recent analyses (Jia et al. 2017; Ma'mun et al. 2018; Yu et al. 2018).

Table 2 Adsorption isothermal parameters and correlation coefficients of Langmuir, Freundlich, and Sips models for MB adsorption onto AgNPs-AC

Langmuir model			Freundlich model			Sips model			
q_m	K_L	R^2	K_F	$1/n$	R^2	$1/n$	q_m	B	R^2
71.29	0.011	0.895	4.424	0.445	0.808	2.123	53.06	2.241	0.935

Table 3 Calculated kinetic parameters of models for adsorption of MB onto AgNPs-AC

Pseudo-first order			Pseudo-second order			Elovich			$q_{e,exp}$ (mg/g)
$q_{m,cal}$ (mg/g)	K_1	R^2	$q_{m,cal}$ (mg/g)	K_2	R^2	α	β	R^2	
173.63	0.039	0.9889	205.25	2.084	0.9741	13.52	0.02	0.9441	172.22

3.6 Effect of Initial MB Concentration

The effects of various initial MB concentrations (C_0) on the adsorption of MB onto AgNPs-AC are shown in Fig. 8. Experiments were conducted by fixing the AgNP-AC amount at 250 mg with a change of initial MB concentrations from 100 to 1000 mg/L at optimum pH of 10. All experiments were done in flasks shaken at 120 rpm for 180 min at room temperature (25 ± 2 °C).

From Fig. 8, adsorption capacity of MB onto AgNPs-AC increased from 7.78 to 64.63 mg/g, which corresponded with an increase in initial MB concentrations from 100 to 1000 mg/L. However, removal efficiency of MB increased from 78 to 90% with low initial MB concentrations, these ranging from 100 to 400 mg/L. Here, the active sites on the adsorbent surface will not be unoccupied at low concentration due to an increase in the driving force for mass transfer (Barka et al. 2011). The percentage of MB removal fell from 88 to 65% by increasing the MB concentration from 500 to 1000 mg/L. This can be explained by the amount of MB increasing while that of adsorbent did not change and active adsorption sites on the AgNP-AC surface were limited.

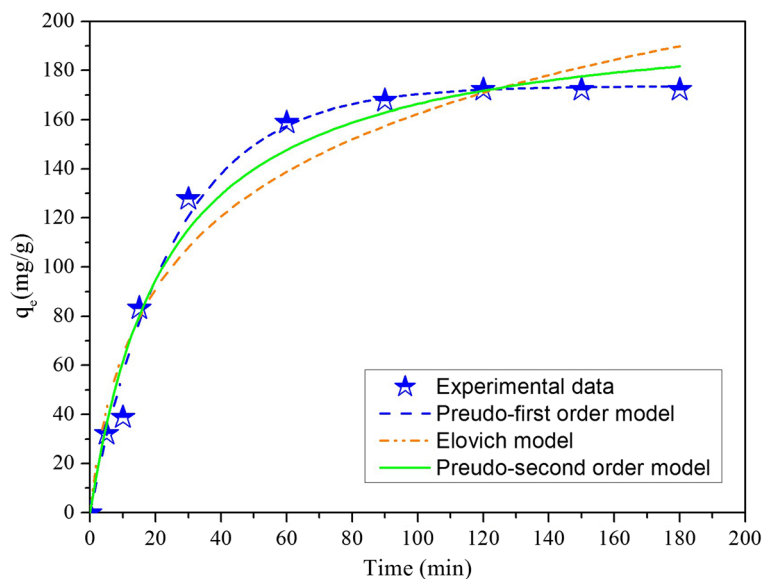
Thus, there were not enough active sites for MB to attach to the AgNP-AC surface (AbdEl-Salam et al. 2017). Similar results have been obtained in other studies (AbdEl-Salam et al. 2017; Shu et al. 2015).

3.7 Adsorption Isotherm

Figure 9 provides a typical adsorption isotherm plot of q_e against C_e . In this study, we applied several commonly adsorption isotherm models to describe the MB adsorption onto AgNPs-AC. They are the Langmuir (Eq. 4), Freundlich (Eq. 5), and Sips (Eq. 6) models. The corresponding parameters of those models are summarized in Table 2.

The adsorption data of MB onto AgNPs-AC were found to fit well to the Langmuir, Freundlich, and Sips models with R^2 values of 0.895, 0.808, and 0.935, respectively. However, the Sips model could better describe the adsorption behaviors of MB onto AgNPs-AC when compared with the Langmuir and Freundlich models. The maximum adsorption capacities (q_m) of AgNPs-AC from the Langmuir and Sips models were calculated to be approximately 71.29 mg/g and

Fig. 10 Kinetic models of MB adsorption onto AgNPs-AC (initial concentration MB, 500 mg/L; adsorbent dosage, 50 mg/25 mL; solution pH, 10; temperature, 25 °C)



53.05 mg/g, respectively. Moreover, the values of the Freundlich exponent ($1/n$) < 1 indicated that the systems were favorable.

3.8 Adsorption Kinetics of MB onto AgNPs-AC

In this study, three common kinetic models were applied to describe the MB adsorption process onto AgNPs-AC, including the pseudo-first-order (PFO; Eq. 7), pseudo-second-order (PSO Eq. 8), and Elovich (Eq. 9) models. The correct application of such selective models was discussed in detail by Vu et al. (2017).

The calculated kinetic parameters in the pseudo-first-order, pseudo-second-order, and Elovich models are shown in Table 3. According to the linear regression coefficient (R^2), the dynamics of MB adsorption fit well to all three models. As shown in Table 3, the pseudo-first-order and pseudo-second-order models provided excellent correlation coefficients ($R^2 = 0.9889$ and 0.9741 , respectively) with the experimental data compared to the Elovich model. The calculated q_m value from the pseudo-first-order and pseudo-second-order model was very close to the experimental data (173.63 and 205.25 mg/g). These results proved that the experimental data followed well the pseudo-first-order and pseudo-second-order models and both models could describe the adsorption kinetics of MB onto AgNPs-AC (Fig. 10). The fitting of experimental data using pseudo-first-order and pseudo-second-order models suggest that adsorption of MB onto AgNPs-AC is controlled by chemisorption, which involves valence forces through sharing or exchange of electrons (Pathania et al. 2017). Thus, the kinetics of MB adsorption on AgNPs-AC were well described by the pseudo-first-order and pseudo-second-order models.

4 Conclusions

In this study, we developed a new and cost-effective adsorbent through loading silver nanoparticles (AgNPs) onto commercial activated carbon (AC) to produce AgNPs-AC for methylene blue (MB) removal from aqueous solution. The characteristics of AgNPs-AC were analyzed by SEM, XRD, and FTIR. Adsorption isotherm and kinetics of MB onto AgNPs-AC were studied using various models, and the findings indicated that coating of AgNPs onto AC increased MB adsorption. The new AgNPs-AC had higher adsorption

capacity for MB than that of commercial-activated carbon because the number active sites increased on the surface of new adsorbent through impregnation of AC by AgNPs. The impregnation ratio of 0.5% proved to be the most suitable scenario. The operating parameters when adsorption capacity reached the highest value were as follows: (i) adsorbent dose of 250 mg/25 mL, (ii) contact time of 120 min at initial MB concentration of 500 mg/L, and (iii) pH of 10. The adsorption isothermal equilibrium is best described by the Sips model. The adsorption kinetic data were found to fit well with the pseudo-first and second-order models with very high correlation coefficients. Finally, the mechanism of adsorption was chemisorption. The material (AgNPs-AC) with the high adsorption capacity (172.22 mg/g) for methylene blue will be the potential sorbent for treatment of persistent organic compounds from wastewater such as textile wastewater and other industrial wastewater. The adsorption method with activated carbon-loaded silver nanoparticles developed in this study can be used to replace the popular method to remove color and the amount of persistent organic compounds in industrial wastewaters with lower cost.

Publisher's Note Springer Nature remains neutral with regard to jurisdictional claims in published maps and institutional affiliations.

References

- AbdEl-Salam, A. H., Ewais, H. A., & Basaleh, A. S. (2017). Silver nanoparticles immobilised on the activated carbon as efficient adsorbent for removal of crystal violet dye from aqueous solutions. A kinetic study. *Journal of Molecular Liquids*, *248*, 833–841.
- Abe, M., Kawashima, K., Kozawa, K., Sakai, H., & Kaneko, K. (2000). Amination of activated carbon and adsorption characteristics of its aminated surface. *Langmuir*, *16*, 5059–5063.
- Altintig, E., Arabaci, G., & Altundag, H. (2016). Preparation and characterization of the antibacterial efficiency of silver loaded activated carbon from corncobs. *Surface and Coatings Technology*, *304*, 63–67.
- Anisuzzaman, S. M., Joseph, C. G., Taufiq-Yap, Y. H., Krishnaiah, D., & Tay, V. V. (2015). Modification of commercial activated carbon for the removal of 2,4-dichlorophenol from simulated wastewater. *Journal of King Saud University - Science*, *27*, 318–330.
- Barka, N., Qourzal, S., Assabbane, A., Nounah, A., & Ait-Ichou, Y. (2011). Removal of reactive yellow 84 from aqueous solutions by adsorption onto hydroxyapatite. *Journal of Saudi Chemical Society*, *15*, 263–267.

- Benaouda, B., Benderdouche, N., Benstaali, B., Mostefa, B. & Addou, A. (2008). Methylene blue and iodine adsorption onto an activated desert plant, 8441–8444 pp.
- Chen, Y., Lin, Y.-C., Ho, S.-H., Zhou, Y. & Ren, N.-q. (2018). Highly efficient adsorption of dyes by biochar derived from pigments-extracted macroalgae pyrolyzed at different temperature.
- Chingombe, P., Saha, B. & J Wakeman, R. (2006). Sorption of atrazine on conventional and surface modified activated carbons, 408–416 pp.
- Dada, A.O., Olalekan, A. & Olatunya, A. (2012). Langmuir, Freundlich, Temkin and Dubinin–Radushkevich isotherms studies of equilibrium sorption of Zn 2+ onto phosphoric acid modified rice husk. 3, 38–45.
- De Castro, M.L.F.A., Abad, M.L.B., Sumalinog, D.A.G., Abarca, R.R.M., Paoprasert, P. & de Luna, M.D.G. (2018). Adsorption of methylene blue dye and Cu (II) ions on EDTA-modified bentonite: isotherm, kinetic and thermodynamic studies. *Sustainable Environment Research*.
- El Alouani, M., Alehyen, S., El Achouri, M., & Taibi, M. (2018). Removal of cationic dye – methylene blue - from aqueous solution by adsorption on Fly Ash - based Geopolymer. *Journal of Materials and Environmental Sciences*, 9, 32–46.
- El Qada, E. N., Allen, S. J., & Walker, G. M. (2008). Adsorption of basic dyes from aqueous solution onto activated carbons. *Chemical Engineering Journal*, 135, 174–184.
- Fierro, V., Torné-Fernández, V., & Celzard, A. (2006). Kraft lignin as a precursor for microporous activated carbons prepared by impregnation with ortho-phosphoric acid: synthesis and textural characterisation. *Microporous and Mesoporous Materials*, 92, 243–250.
- Foo, K. Y., & Hameed, B. H. (2009). Utilization of biodiesel waste as a renewable resource for activated carbon: application to environmental problems. *Renewable and Sustainable Energy Reviews*, 13, 2495–2504.
- Ganau, M., Paris, M., Syrmos, N., Ganau, L., Ligarotti, G., Moghaddamjou, A., Prisco, L., Ambu, R., & Chibbaro, S. (2018). How nanotechnology and biomedical engineering are supporting the identification of predictive biomarkers in neuro-oncology. *Medicines*, 5, 23.
- Ghosh, D., & Bhattacharyya, K. G. (2002). Adsorption of methylene blue on kaolinite. *Applied Clay Science*, 20, 295–300.
- Hamadi, A. A., Uraz, G., Ö, H.K.a, & Osmanağaoğlu. (2017). Adsorption of Azo Dyes from Textile Wastewater by *Spirulina Platensis*. *Eurasian Journal of Environmental Research*, 1, 19–27.
- Jia, P., Tan, H., Liu, K., & Gao, W. (2017). Adsorption behavior of methylene blue by bone char. *International Journal of Modern Physics B*, 31, 1744099.
- Krishnananda, P. I., Amit, G. D., Dipika, A. P., Mahendra, S. D., Mangesh, P. M., & VC, K. (2017). Silver nanoparticles: a new era of nanobiotechnology. *The Pharma Innovation Journal*, 6, 1–4.
- Kritika, B., Shruti, S., Jyoti, P., & Pawan, I. (2010). Recent developments in electronics under nanotechnology-nanoelectronics. *International Journal of Electronics and Computer Science Engineering*, 1, 2398–2403.
- Kushwaha, A. K., Gupta, N., & Chattopadhyaya, M. C. (2014). Removal of cationic methylene blue and malachite green dyes from aqueous solution by waste materials of *Daucus carota*. *Journal of Saudi Chemical Society*, 18, 200–207.
- Lazim, Z. M., Hadibarata, T., Puteh, M. H., & Yusop, Z. (2015). Adsorption characteristics of bisphenol a onto low-cost modified phyto-waste material in aqueous solution. *Water, Air, & Soil Pollution*, 226.
- Lopes, A. S.d. C., Carvalho, S. M. L.o.d., Brasil, D.d. S. B., Mendes, R.d. A., & Lima, M. O. (2015). Surface modification of commercial activated carbon (CAG) for the adsorption of benzene and toluene. *American Journal of Analytical Chemistry*, 528–538.
- Ma'mun, S., Siswoyo, E., Adrian, A. R., Tanaka, S., Tamura, H., & Purnomo, M. R. A. (2018). Bioadsorbent based on water hyacinth modified with citric acid for adsorption of methylene blue in water. *MATEC Web of Conferences*, 154, 01012.
- Mulfinger, L., Solomon, S. D., Bahadory, M., Jeyarajasingam, A. V., Rutkowsky, S. A., & Boritz, C. (2007). Synthesis and study of silver nanoparticles. *Journal of Chemical Education*, 84, 322.
- Nguyen, T. C., Loganathan, P., Nguyen, T. V., Vigneswaran, S., Kandasamy, J., & Naidu, R. (2015). Simultaneous adsorption of Cd, Cr, Cu, Pb, and Zn by an iron-coated Australian zeolite in batch and fixed-bed column studies. *Chemical Engineering Journal*, 270, 393–404.
- Özbay, N., Yargıç, A. Ş., Yarbay-Şahin, R. Z., & Önal, E. (2013). Full factorial experimental design analysis of reactive dye removal by carbon adsorption. *Journal of Chemistry*, 2013, 1–13.
- Pathania, D., Sharma, S., & Singh, P. (2017). Removal of methylene blue by adsorption onto activated carbon developed from *Ficus carica* bast. *Arabian Journal of Chemistry*, 10, S1445–S1451.
- Rafatullah, M., Sulaiman, O., Hashim, R. & Ahmad, A. (2010). Adsorption of methylene blue on low-cost adsorbents: a review, 70–80 pp.
- Raposo, F., De La Rubia, M. A., & Borja, R. (2009). Methylene blue number as useful indicator to evaluate the adsorptive capacity of granular activated carbon in batch mode: influence of adsorbate/adsorbent mass ratio and particle size. *Journal of Hazardous Materials*, 165, 291–299.
- Rice, E. W., Baird, R. B., Eaton, A. D., & Clesceri, L. S. (2012). *Standard methods for the examination of water and wastewater*. Washington DC: American Public Health Association.
- Salem, I. A., Fayed, T. A., El-Nahass, M. N., & Dawood, M. (2018). A comparative study for adsorption of methylene blue dye from wastewater on to three different types of Rice Ash. *Journal of Pharmaceutical and Applied Chemistry*, 4, 99–107.
- Sara, D., & Tushar, K. S. (2014). Review on dye removal from its aqueous solution into alternative cost effective and non-conventional adsorbents. *Journal of Chemical and Process Engineering*, 1, 1–11.
- Sharma, Y.C. & Sharma, U. (2010). Optimization of parameters for adsorption of methylene blue on a low-cost activated carbon.
- Shu, J., Wang, Z., Huang, Y., Huang, N., Ren, C., & Zhang, W. (2015). Adsorption removal of Congo red from aqueous solution by polyhedral Cu₂O nanoparticles: kinetics, isotherms, thermodynamics and mechanism analysis. *Journal of Alloys and Compounds*, 633, 338–346.
- Singh, C. K., Sahu, J. N., Mahalik, K. K., Mohanty, C. R., Mohan, B. R., & Meikap, B. C. (2008). Studies on the removal of Pb (II) from wastewater by activated carbon developed from

- Tamarind wood activated with sulphuric acid. *Journal of Hazardous Materials*, 153, 221–228.
- Stoyanova, M., & Christoskova, S. (2011). Catalytic degradation of methylene blue in aqueous solutions over Ni- and Co-oxide systems. *Open Chemistry*, 1000.
- Syu, Y.-Y., Hung, J.-H., Chen, J.-C. & Chuang, H.-w. (2014). Impacts of size and shape of silver nanoparticles on Arabidopsis plant growth and gene expression, 57–64 pp.
- Tan, I. A. W., Ahmad, A. L., & Hameed, B. H. (2008a). Adsorption of basic dye on high-surface-area activated carbon prepared from coconut husk: equilibrium, kinetic and thermodynamic studies. *Journal of Hazardous Materials*, 154, 337–346.
- Tan, I. A. W., Ahmad, A. L., & Hameed, B. H. (2008b). Adsorption of basic dye using activated carbon prepared from oil palm shell: batch and fixed bed studies. *Desalination*, 225, 13–28.
- Tan, K.A., Morad, N., Teng, T.T., Ismail, N. & Perumal, P. (2012). Removal of cationic dye by magnetic nanoparticle (Fe₃O₄) impregnated onto activated maize cob powder and kinetic study of dye waste adsorption, 83–89 pp.
- Tang, C., Hu, D., Cao, Q., Yan, W., & Xing, B. (2017). Silver nanoparticles-loaded activated carbon fibers using chitosan as binding agent: preparation, mechanism, and their antibacterial activity. *Applied Surface Science*, 394, 457–465.
- Tran, H. N., You, S.-J., & Chao, H.-P. (2015). Effect of pyrolysis temperatures and times on the adsorption of cadmium onto orange peel derived biochar. *Waste Management & Research*, 34, 129–138.
- Vaiopoulou, E., & Gikas, P. (2011). Effects of chromium on activated sludge and on the performance of wastewater treatment plants: a review. In 549–570 pp.
- Vu, T. M., Trinh, V. T., Doan, D. P., Van, H. T., Nguyen, T. V., Vigneswaran, S., & Ngo, H. H. (2017). Removing ammonium from water using modified corn-cob-biochar. *Science of the Total Environment*, 579, 612–619.
- Yorgun, S., Vural, N., & Demiral, H. (2009). Preparation of high-surface area activated carbons from Paulownia wood by ZnCl₂ activation. *Microporous and Mesoporous Materials*, 122, 189–194.
- Yu, J., Zhang, X., Wang, D., & Li, P. (2018). Adsorption of methyl orange dye onto biochar adsorbent prepared from chicken manure. *Water Science and Technology*, 77, 1303–1312.